# Loss of the Hematopoietic Stem Cell Factor GATA2 in the Osteogenic Lineage Impairs Trabecularization and Mechanical Strength of Bone

Tolkachov, Alexander

2018-06

Tolkachov , A , Fischer , C , Ambrosi , T H , Bothe , M , Han , C-T , Muenzner , M , Mathia , S , Salminen , M , Seifert , G , Thiele , M , Duda , G N , Meijsing , S H , Sauer , S , Schulz , T J & Schupp , M 2018 , ' Loss of the Hematopoietic Stem Cell Factor GATA2 in the Osteogenic Lineage Impairs Trabecularization and Mechanical Strength of Bone ' , Molecular and Cellular Biology , vol. 38 , no. 12 , UNSP e00599-17 . https://doi.org/10.1128/MCB.00599-17

http://hdl.handle.net/10138/238981
https://doi.org/10.1128/MCB.00599-17

unspecified
acceptedVersion

# Loss of the hematopoietic stem cell factor GATA2 in the osteogenic lineage impairs trabecularization and mechanical strength of bone

Running Title: GATA2 in bone homeostasis

Alexander Tolkachov,[a] Cornelius Fischer,[b] Thomas H. Ambrosi,[c,d] Melissa Bothe,[e] Chung-Ting Han,[b,*] Matthias Muenzner,[a] Susanne Mathia,[f] Marjo Salminen,[g] Georg Seifert,[h] Mario Thiele,[i] Georg N. Duda,[i] Sebastiaan H. Meijsing,[e] Sascha Sauer,[b] Tim J. Schulz,[c,d] and Michael Schupp[a#]

[a]Charité-Universitätsmedizin Berlin, corporate member of Freie Universität Berlin, Humboldt-Universität zu Berlin, and Berlin Institute of Health, Institute of Pharmacology, Berlin, Germany

[b]Laboratory of Functional Genomics, Nutrigenomics and Systems Biology, BIMSB and BIH Genomics Platforms, Max-Delbrück-Center for Molecular Medicine, Berlin, Germany.

[c]Research Group Adipocyte Development, German Institute of Human Nutrition (DlfE), Potsdam-Rehbrucke, Nuthetal, Germany

[d]German Center for Diabetes Research (DZD), München-Neuherberg, Germany

[e]Max Planck Institute for Molecular Genetics, Berlin, Germany

[f]Charité-Universitätsmedizin Berlin, corporate member of Freie Universität Berlin, Humboldt-Universität zu Berlin, and Berlin Institute of Health, Nephrology and Renal Transplantation, Berlin, Germany

[g]Department of Veterinary Biosciences, University of Helsinki, Helsinki, Finland

[h]Charité-Universitätsmedizin Berlin, corporate member of Freie Universität Berlin, Humboldt-Universität zu Berlin, and Berlin Institute of Health, Department of Pediatric Oncology/ Hematology, Otto-Heubner-Center for Pediatric and Adolescent Medicine, Berlin, Germany

[i]Charité-Universitätsmedizin Berlin, corporate member of Freie Universität Berlin, Humboldt-Universität zu Berlin, and Berlin Institute of Health, Julius Wolff Institute and Berlin-Brandenburg School for Regenerative Therapies, Berlin, Germany

[#]Address correspondence to Michael Schupp, michael.schupp@charite.de.

[*]Present address: CeGaT GmbH, Center for Genomics and Transcriptomics, Tübingen, Germany

Word count abstract: 156

Word counts manuscript text: 4,934

(Abstract, Introduction, Results, Discussion, and Figure legends)

## ABSTRACT

The transcription factor GATA2 is required for expansion and differentiation of hematopoietic stem cells (HSCs). In mesenchymal stem cells (MSCs) GATA2 blocks adipogenesis, but its biological relevance and underlying genomic events are unknown. We report a dual function of GATA2 in bone homeostasis. GATA2 in MSCs binds near genes involved in skeletal system development and co-localizes with motifs for FOX and HOX transcription factors, known regulators of skeletal development. Ectopic GATA2 blocks osteoblastogenesis by interfering with SMAD1/5/8 activation. MSC-specific deletion of GATA2 in mice increases numbers and differentiation capacity of bone-derived precursors, resulting in elevated bone formation. Surprisingly, MSC-specific GATA2 deficiency impairs trabecularization and mechanical strength of bone, involving reduced MSC expression of the osteoclast inhibitor osteoprotegerin and increased osteoclast numbers. Thus, GATA2 affects bone turnover via MSC-autonomous and indirect effects. By regulating bone trabecularization, GATA2 expression in the osteogenic lineage may contribute to the anatomical and cellular microenvironment of the HSC niche required for hematopoiesis.


## INTRODUCTION

GATA2 belongs to a family of six structurally related zinc finger transcription factors (GATA1-6) and plays a critical role in hematopoiesis. Mice that lack GATA2 die during embryonic development due to severe anemia upon impaired proliferation and survival of early hematopoietic stem cells (HSCs) (1). Expression of GATA2 in HSCs is required for the expansion of multipotent hematopoietic cells and the formation of mast cells, but was found dispensable for the terminal differentiation of erythroid cells and macrophages (2). In humans, germline mutations in GATA2 are associated with the GATA2-deficiency syndrome, which manifests as a complex array of hematologic, neoplastic, dermatologic, and pulmonary symptoms that can be accompanied by certain viral infections and congenital deafness (3).

66 Acquired mutations have been linked to myelodysplastic syndrome, acute myeloid leukemia,
67 and to blast crisis transformation of chronic myeloid leukemia (4).
68
69 Besides its expression in hematopoietic precursors, GATA2 is expressed in mesenchymal
70 stem/stromal cells (MSCs) (5), common precursors for *e.g.* adipocytes, myocytes, osteocytes
71 and chondrocytes. In part owing to the embryonic lethality of GATA2-deficient mice,
72 GATA2's function in MSCs is much less investigated and most insights derive from studying
73 its role during adipogenesis. GATA2 was shown to block differentiation of both white and
74 brown precursor cells (5-7) by reducing peroxisome proliferator-activated receptor γ (PPARγ)
75 promoter activity and by interfering with CCAAT/enhancer binding protein (C/EBP)-
76 mediated transcription (8).
77
78 Here, we report the first genome-wide analysis of GATA2 binding sites in mesenchymal cells
79 and implicate this transcription factor in bone homeostasis. GATA2 binds canonical motifs
80 near genes involved in skeletal development and blocks osteoblastogenesis. Mice that lack
81 GATA2 specifically in MSCs developed normally but, surprisingly, showed reduced bone
82 trabecularization and bone strengths involving lower osteoprotegerin (*Opg*) expression in
83 MSCs and higher osteoclast numbers. Moreover, MSC-specific deletion of GATA2 reduced
84 red blood cell counts which may imply a much broader role for GATA2 in the control of
85 hematopoiesis than previously thought.
86
87 **RESULTS**
88 **GATA2 regulates and binds the Zfpm1 gene in mesenchymal 3T3-L1 cells.** GATA factors
89 regulate gene expression via their interaction with friend of gata (FOG)/zinc finger protein,
90 FOG family member (ZFPM) cofactors (9). ZFPM1 is also a transcriptional target of GATA
91 factors in hematopoietic cells, and binding sites near the *Zfpm1* gene locus (+0.7 and +24.4 kb

of the transcriptional start site (TSS)) have been previously identified in G1E-ER cells, an erythroid cell line (10). We focused on *Zfpm1* in order to identify a functionally relevant binding site of GATA2 in 3T3-L1 cells, an adipocyte-lineage committed mesenchymal cell line (11). As previously reported (6, 12), GATA2 is down-regulated during adipogenesis (Fig. 1A, before (day 0) and 14 days after the initiation of differentiation). Similarly, mRNA expression of *Zfpm1* was reduced (Fig. 1B) in accordance with a recent study (13), suggesting that GATA2 regulates *Zfpm1* expression in 3T3-L1 cells. Indeed, retroviral over-expression of GATA2 in preadipocytes up-regulated ZFPM1 protein (Fig. 1C). We performed chromatin immunoprecipitation (ChIP) of endogenous GATA2 and found that binding was conserved at +0.7 kb but not +24.7 kb of the *Zfpm1* TSS in 3T3-L1 cells and absent in adipocytes (Fig. 1D), consistent with the low expression of GATA2 after differentiation. An upstream site (-1.4 kb) served as negative control. GATA2 binding to +0.7 kb of *Zfpm1* was used as control/validation site for all further ChIP experiments. Input and GATA2-enriched chromatin of undifferentiated 3T3-L1 cells (>5 fold enriched at +0.7 of *Zfpm1*) was subjected to high-throughput sequencing (ChIP-seq).

**GATA2 binds genomic WGATAR motifs and is enriched at skeletal development genes.** We identified a total of 1,975 peaks (false discovery rate (FDR) 1%) (Table S1) and more than 90% localized to intergenic and intronic regions. Only a small fraction mapped to proximal promoters (73 peaks within 3 kb 5' of the TSS) (Fig. 1E). Binding to five randomly selected sites near the genes *Prickle*, *Tinag*, *Cdk4*, *Tsen* and *RetSat* was validated and confirmed by ChIP-qPCR (data not shown). *De novo* motif analysis of genome-wide GATA2 binding sites by SeqPos (14) revealed that GATA containing sequences represented the top three motif clusters (Fig. 1F, + and – strands), matching the consensus WGATAR motif (W=T or A; R=G or A) (15-17) to a high extent. Of note, also E- box motifs of (CANNTG)-WGATAR-containing composite elements, known to be important for GATA's cooperative

function with other transcription factors (16, 18), were enriched although much less significantly (Fig. 1G, top panel). Interrogating known binding motifs in peak regions identified either GATA factors or transcription factors with binding motifs that contain GATA (Fig. 1G, bottom panel). Binding sites showed evolutionary conservation when assessed by phastCons, which is based on a two-state phylogenetic hidden Markov model (19) (Fig. 1H). Next, nearby genes (located 70 kb 5`or 3`of GATA2 binding sites, n=2,230 genes, Table S2) were analyzed by gene ontology analysis and enriched to pathways involving transcription, nucleic acids, and nitrogen compound metabolic process (Fig. 1I). Strikingly, one of the top-ranking pathways mapped to skeletal system development (Fig. 1I, n=56 genes, Table S2), suggesting a role for GATA2 in osteoblast differentiation and bone homeostasis. Binding to six randomly selected sites near genes of this pathway (*Foxc2*, *Cobl*, *Sfrp2*, *Igsf10*, *Man2a1* and *Ptgs2*) was validated and confirmed by ChIP-qPCR (data not shown).

**HSC versus MSC-specific binding of GATA2.** We then intersected the 3T3-L1 GATA2 cistrome with a published data set of GATA2 binding sites in FDCPmix cells (20), a bone marrow-derived cell line with HSC-like characteristics (21). The number of peaks/binding sites (Table S1) and nearby genes (Table S2) were much higher in these cells (FDR 1%) and overlapped with about 54% of the genes within 70 kb of GATA2 binding in 3T3-L1 cells (Fig. 2A). 3T3-L1-specific, overlapping and mHSC-specific genomic GATA2 binding sites were mapped to H3K4me1, H3K27ac, and chromatin DNase I hypersensitivity sequencing (DHS) data of 3T3-L1 preadipocytes (Fig. 2B). We found strong enrichment of H3K4me1 and H3K27ac on both 3T3-L1-specific and overlapping GATA2 binding sites, whereas DHS was strongest on overlapping sites, followed by 3T3-L1 and mHSC-specific sites. These results support the notion that cell-type specific chromatin accessibility determines GATA2 binding. Moreover, when analyzed separately for gene ontology, 'embryonic skeletal system morphogenesis' and 'development' were now the two top ranking pathways of genes located

144 near GATA2 sites that are specific to 3T3-L1 cells (n=1,011 genes), whereas both
145 overlapping genes (n=1,219 genes) and genes near HSC-specific binding sites (n=6,316)
146 mapped to other, skeletal system-unrelated pathways (Fig. 2C, left panel, corresponding genes
147 in Table S2). We then asked which motifs besides WGATAR enrich to cell type-specific
148 peaks. Motifs for transcription factors of the FOX and HOX family, known regulators of
149 neural crest cells and skeletal development (22, 23) were found near 3T3-L1-specific,
150 whereas motifs for a variety of factors involved in hematopoiesis were identified near HSC-
151 specific binding sites (Fig. 2C, right panel). Thus, GATA2 appears to co-localize with
152 specific lineage-determining transcription factors that may prime and/or facilitate cell type-
153 selective binding. GATA2 binding sites near *Zfpm1* and *Ccna1* were conserved in
154 C3H10T1/2 cells (Fig. 2D, left panel) that, in contrast to adipocyte lineage-committed 3T3-L1
155 cells, are mesenchyme-derived cells that exhibit multipotency (24). GATA2 ChIP-seq in these
156 cells identified 1,517 binding sites (FDR 1%) (Table S1) and the GATA consensus motif as
157 the most enriched sequence (Fig. 2D, right panel top). Of the 1,936 genes located near
158 GATA2 binding sites in C3H10T1/2 cells (Table S2), 989 overlapped with those in 3T3-L1
159 (Fig. 2D, right panel bottom). As expected, heatmap visualization showed a much higher
160 overlap of GATA2 binding sites between the two mesenchymal cell lines compared to
161 binding in HSCs (Fig. 2E).
162
163 **GATA2 blocks osteoblastogenesis and impairs SMAD signaling.** To test the hypothesis
164 that GATA2 regulates osteoblast differentiation, we retrovirally over-expressed GATA2 in
165 C3H10T1/2 cells (Fig. 3A) and stimulated osteoblastic conversion. Remarkably, ectopic
166 GATA2 strongly suppressed osteoblastogenesis, when assessed by alkaline phosphatase
167 (ALPL) staining, Alizarin staining of calcium deposition, and by the expression of osteoblast
168 marker genes after 8 days of differentiation (Fig. 3B and 3C, respectively). Since Wnt- and
169 SMAD-signaling are pivotal in controlling osteoblast differentiation (25, 26), we tested

whether ectopic GATA2 would interfere with these pathways. GATA2 blocked the BMP2-induced activation of a SMAD1/5/8 luciferase reporter (Fig. 3D) but had no discernable effect on basal or the LiCl-mediated activation of a Wnt-reporter system (Fig. 3E). We then isolated $Lin^-$ $Sca1^+$ MSCs from subcutaneous white adipose tissue (sqWAT) and ectopically expressed GATA2 in these primary cells (Fig. 3F). Affymetrix gene expression-profiling showed that ectopic expression of GATA2 in undifferentiated cells regulated 805 of the 2,230 genes with nearby GATA2 binding (Table S3) and 41 of 102 ($q < 0.05$) genes defined by the GO terms related to skeletal system development (Fig. 3G, Table S2), and several SMAD's and respective target genes (Fig. 3H). Since the majority of these genes were down-regulated (n=29 vs. 12), GATA2 seems to function primarily as a repressor of genes involved in skeletal development/osteoblast differentiation. Moreover, GATA2 also potently inhibited osteoblastogenesis in primary MSCs as shown by reduced ALPL and Alizarin staining and lower expression of osteoblast marker genes after 8 days of differentiation (Fig. 3I and 3J). Taken together, GATA2 inhibits osteoblastogenesis of MSCs, at least in part, by interfering with genes related to skeletal development such as BMP2-driven SMAD-signaling.

**MSC-specific GATA2 deletion increases precursor cell numbers in bone and enhances *in vitro* osteoblastogenesis.** We then addressed the effects of GATA2 deficiency by crossing mice with floxed *Gata2* alleles (27) with Prx1-Cre mice deleting specifically in MSCs but not $CD45^+$ hematopoietic or $CD31^+$ endothelial cell populations (28, 29). This strategy allowed deletion in MSCs derived from bone and sqWAT, but not in those of eWAT or brown adipose tissue (BAT) (Fig. 4A), consistent with previous reports on the Prx1-Cre line (30, 31). Notably, GATA2 deletion was not detectable when analyzing whole tissue mRNA, presumably due to GATA2 expression in cell types that are not targeted by Prx1-Cre (data not shown). Loss of GATA2 in sqWAT MSCs was confirmed on protein level (Fig. 4B) and did not induce an up-regulation of other GATA family members as a compensational response

(Fig. 4C). We found that GATA2 deletion increased the number of bone-resident Lin$^-$ Sca1$^+$ and Lin$^-$ Sca1$^-$ Pdgfra$^+$ MSCs (Fig. 4D), precursor populations with high adipogenic and osteoblastogenic capacity, respectively (29). When assessed for *in vitro* osteoblast differentiation by Alizarin staining and the expression of osteoblast marker genes, adipogenic Lin$^-$ Sca1$^+$ cells lacking GATA2 showed a striking enhancement of osteoblast differentiation (Fig. 4E and 4F) whereas there was no difference in the differentiation of Lin$^-$ Sca1$^-$ Pdgfra$^+$ MSCs (Fig. 4G and 4H). Thus, deletion of GATA2 increases the numbers of bone-residing precursor cells and enhances the osteoblastic potential of Lin$^-$ Sca1$^+$ precursors. Interestingly and in contrast to bone, GATA2 deletion in sqWAT-resident MSCs did not affect Lin$^-$ Sca1$^+$ or Lin$^-$ Sca1$^-$ cell numbers, sqWAT tissue mass, or *in vitro* adipogenesis of Lin$^-$Sca1$^+$ cells, when assessed by Oil Red O lipid staining and the expression of adipocyte marker genes (data not shown).

**MSC-specific GATA2 deletion impairs trabecularization and mechanical strength of bone.** We next analyzed bone structure of mice with MSC-specific GATA2 deletion and found no differences in cartilage or bone morphogenesis of day E18.5 fetuses (Fig. 5A, top panel), or in growth plate morphology/ height (Fig. 5A, bottom panels) and tibia length (17.6 ± 0.23 mm in Cre (-) vs. 17.8 ± 0.14 mm in Cre (+), n=4,4) at three months of age. However, µCT analyses revealed a profound impairment of tibial trabecularization in the transitional section from the meta- to the diaphysis of three months old mice (Fig. 5B) with bone surface and trabeculae numbers strongly reduced (Fig. 5C). This observation was surprising and opposite to the phenotype we would have predicted from our findings regarding the increase in numbers and osteoblastic potential of bone-resident MSCs. Three-point bone bending, which depends predominantly on mid-diaphysis structure, showed that femora of aged mice with MSC-specific GATA2 deletion exhibited reduced cortical strength (Fig. 5D). To determine whether increased MSC numbers (Fig. 4D) could improve bone regeneration, we

assessed healing of a stabilized tibia fracture histomorphometrically but found no significant differences in mineralized and cartilaginous tissues between genotypes that would point towards an altered healing process (data not shown). Hence, GATA2 expression in bone-resident MSCs is required for bone trabecularization and its cortical strength but dispensable for the regeneration of fractured bone.

**MSC-specific GATA2 deletion activates osteoclasts involving reduced osteoprotegerin and alters blood cell counts.** In order to identify the reason for impaired trabecularization in mice with MSC-specific GATA2 deletion, we first investigated bone anabolism and determined mineral apposition rate (MAR) by calcein double staining. MSC-specific deletion of GATA2 increased MAR in trabecular bone (Fig. 6A) whereas there was no effect in cortical bone (data not shown). This indicates that reduced trabecularization is unlikely due to reduced bone formation. We next assessed whether differentiation of GATA2-deficient bone-resident MSCs shifted towards adipocytes and found that *in vitro* adipogenesis of bone-derived $Lin^-$ $Sca1^+$ cells was indeed enhanced (increased Oil Red staining and mRNA expression of the adipogenic marker genes *Ppar*$\gamma_2$ (18.7 ± 1.99 fold) , *Cebpa* (6.8 ± 0.92 fold), *aP2* (33.5 ± 2.26 fold) in Cre (+) compared to Cre (-) cells, after the induction of differentiation). In contrast, H&E staining of bone sections and mRNA expression of adipocyte marker genes in bone failed to support a significant increase in bone marrow adipocytes (data not shown). Instead, bone mRNA expression of osteoclast marker genes and the number of osteoclasts determined as tartrate-resistant acid phosphatase (TRAP)-positive, multinucleated cells was increased (Fig. 6B and 6C). This suggests that impaired trabecularization could be caused by an imbalance of catabolic over anabolic bone cells. Since GATA2 deletion in these mice is specific to the mesenchymal lineage, we analyzed known osteoblast-derived signals that affect osteoclast differentiation and activity. Expression of receptor activator of nuclear factor kappa B ligand (*Rankl*) (32, 33) and colony stimulating

factor 1 (*Csf1*) (34) were unchanged in bone of GATA2-deleted mice, whereas that of *Opg* (35) was reduced by 50% (Fig. 6D). Since OPG is a decoy receptor for the osteoclast-differentiation factor RANKL (36, 37), this gene expression pattern is consistent with the observed increase in osteoclasts. Thus, reduced trabecularization may be a consequence of lower expression of *Opg* and increased osteoclast differentiation. To investigate whether *Opg* is a direct transcriptional target of GATA2 in MSCs, we analyzed GATA2 binding near its genomic locus and found two binding sites at 13.0 and 75.4 kb upstream of its TSS in C3H10T1/2 cells but not in HSCs (Fig. 6E, validated by ChIP-qPCR in Fig. 6F). Deleting GATA2 by adenoviral Cre expression reduced *Opg* expression in bone-derived *Gata2* (flox/flox) $Lin^-$ $Sca1^+$ MSCs (Fig. 6G). A similar down-regulation was observed in mouse embryonic fibroblasts (MEFs) and in $Lin^-$ $Sca1^+$ MSCs derived from sqWAT in an adenoviral Cre-dose and time-dependent manner (data not shown), indicating that the regulation of *Opg* by GATA2 is cell-autonomous and conserved between different mesenchymal cell types. To address whether altered morphology and metabolism of trabecular bone of mice with MSC-specific GATA2 deletion affects hematopoiesis, we analyzed blood parameters. GATA2 deletion caused a slight reduction in red blood cell count and hemoglobin levels whereas there was no difference in the numbers of white blood cells and platelets (Fig. 6H).

## DISCUSSION

In this study, we provide the first genome-wide analysis of GATA2 binding sites in mesenchymal cells and identify a novel function of this transcription factor in establishing bone trabecularization. The most common sequences in genomic regions enriched by GATA2 resemble the canonical WGATAR motif, suggesting that GATA2 affects transcription in these cells predominantly via direct DNA binding rather than being tethered to other transcription factors like C/EBPs (8), or as component of recently identified mega transcription factor complexes (38). Binding sites in MSCs, but not in HSCs, were enriched

near genes involved in skeletal system development and morphogenesis, and co-localized with binding motifs of the FOX and HOX family of transcription factors. This suggests that certain lineage determining factors pioneer for MSC-specific GATA2 binding at short recognition sequences such as the WGATAR motif that occurs in the genome rather frequently. Since MSC-specific, but not HSC-specific GATA2 binding sites associated strongly with H3K4me1 and H3K27ac in mesenchymal cells, chromatin accessibility could account for cell type-specific binding.

Enrichment of binding sites near genes involved in skeletal system development and morphogenesis prompted us to explore GATA2's role during osteoblast differentiation. Indeed, we found that ectopic expression of GATA2 inhibited, whereas genetic deletion of GATA2 in $Lin^-$ $Sca1^+$ precursor cells enhanced osteoblast differentiation, at least in part by interfering with BMP-driven SMAD signaling. Besides osteoblast differentiation, MSC-specific GATA2 deletion also increased the number of mesenchymal precursor cells in bone and enhanced adipocyte differentiation of $Lin^-$ $Sca1^+$ precursor cells *in vitro*. Thus, GATA2's function is to limit precursor cell numbers in bone and the osteoblastic/adipogenic differentiation of certain precursor populations. Intriguingly, deletion of GATA2 in sqWAT-residing precursors did not affect precursor numbers, their adipogenic differentiation, or sqWAT mass, suggesting that GATA2 is biologically more relevant for proliferation and differentiation of MSCs in bone, rather than for those residing in WAT.

At first we were surprised that MSC-specific deletion of GATA2, despite increased numbers of bone-residing precursor cells and enhanced osteoblast differentiation, led to reduced bone trabecularization and lower mechanical strength of bone. Bone formation within trabecular sections was increased but accompanied by elevated numbers of osteoclasts, suggesting that anabolic but also catabolic processes were activated upon loss of GATA2 in MSCs. Our

finding that GATA2 is required for full expression of the osteoclastogenesis inhibitor *Opg* in bone and MSCs, including bone-derived $Lin^-$ $Sca1^+$ precursors, suggests that MSC-specific loss of GATA2 shifts the balance of anabolism versus catabolism within certain bone sections towards catabolism, thus interfering with trabecularization. This is further supported by the phenotype of *Opg* deficient mice that display a similar but much more severe trabecular impairment and cortical bone porosity (39, 40). Since osteoclasts are derived from HSCs and GATA2-deficient osteoclast precursor cells exhibit reduced proliferation (41-43), GATA2 controls osteoclastogenesis not only in a direct and cell-autonomous manner, but also indirectly- via the regulation of *Opg* expression from cells of the mesenchymal lineage. Another interesting observation is that *Opg* deficiency in mice causes hearing loss (44), suggesting that deafness due to mutation of *GATA2* in humans (3) could involve reduced *OPG* expression. Moreover, mutated *OPG* in humans can result in defective vestibular morphology (45), and malformations in similar structures have been found in GATA2 deficient mice (27). Notably, other signals of the osteoblasts and osteoclasts crosstalk may be affected by loss of GATA2 in MSCs and thereby involved in the observed phenotype. Further research is needed to elucidate the contribution of these factors.

Our study is in accordance with some of the findings of Li *et al.* (46), who observed increased osteoblastogenesis of GATA2-deficient MSCs derived from bone. Mechanistically, this was attributed to increased Wnt/β-catenin signaling (46), a pathway whose activity we found not affected by ectopic GATA2 expression. Both Li *et al.* and Kamata *et al.* observed reduced MSC proliferation upon loss of GATA2 or siRNA-mediated depletion of GATA2 in human MSCs (5), respectively. In contrast, we found increased numbers of bone-residing precursor cells in mice with MSC-specific deletion of GATA2, suggesting that MSC proliferation may be influenced by the bone microenvironment. The most striking difference is in regard to reduced trabecularization, since Li *et al.* reported the opposite finding of higher bone mass

and trabecularization upon the loss of GATA2 in MSCs, despite using the same genetic mouse model (46). The reason for this is currently unknown but may involve the spatial stratifications we applied to our µCT analyses. Moreover, Li *et al.* found increased bone marrow adiposity whereas we and others (47) did not, which is another aspect that requires further studies to consolidate these contradictory results.

An intriguing notion concerns the expression of GATA2 in different developmental lineages and why GATA2, as one of the master regulators of HSC differentiation, controls mesenchymal precursors especially in bone. A plausible hypothesis could derive from the greatly advanced understanding of the adult marrow HSC niche (48), where both hematopoietic and mesenchymal cells warrant HSC self-renewal, proliferation, and differentiation (49). GATA2 expression in HSCs is required for their expansion and the formation of mast cells, whereas GATA2 in MSCs may support developing the anatomical and cellular microenvironment of the niche. The slight reduction in red blood cell counts upon MSC-specific GATA2 deletion could be secondary to reduced bone trabecularization and an impaired HSC niche. Notably, accelerated osteoclastogenesis and osteoporosis in *Opg*-deficient mice was accompanied by reduced HSC mobilization and colony formation (50), supporting a link between higher osteoclast number/activity, the microenvironment of the niche, and blood cell formation. Support for a role of GATA2 comes from a study that identified compromised colony formation of hematopoietic progenitor cells from mice lacking GATA2 in MSCs and lower numbers of common myeloid progenitors after the transplantation of $CD45^{+}$ cells into mice that lacked GATA2 in bone marrow (47). On the other hand, lower *Opg* expression upon GATA2 deletion in MSCs could directly hinder HSC expansion since OPG was shown to enhance the expansion of hematopoietic progenitor cells *in vitro* (51). These observations warrant further research to complete our understanding of the interconnection of lineage-specific actions of GATA2.

In summary, we have identified genome-wide binding sites of GATA2 in mesenchymal cells and a novel function of GATA2 in bone trabecularization and mechanical strength, suggesting that GATA2-deficiency syndrome patients may be more vulnerable to bone fractures. Moreover, our study could imply a therapeutic potential of correcting an abnormal skeletal system and bone morphology to treat certain blood diseases.

## MATERIAL AND METHODS

### *Mouse experiments*

All experimental animal procedures were in accordance with institutional guidelines and approved by the 'Landesamt für Gesundheit und Soziales' in Berlin, Germany. Mice were housed under 12/12 hours light/dark cycles and fed standard chow (ssniff R/M-H). C57BL/6 females with floxed *Gata2* alleles (27) were mated with male B6.Cg-Tg(*Prrx1*-cre)1Cjt/J (28) (Jackson laboratory, stock nr. 005584) for deletion in MSCs. Male mice were used for experiments.

### *Culture and differentiation of cell lines*

C3H10T1/2 and 3T3-L1 cells (ATCC) were cultured according to the provider's instructions. 3T3-L1 cells were differentiated to adipocytes by incubation with insulin, dexamethasone, and 3-isobutyl-1-methylxanthine as previously described (52). C3H10T1/2 cells were differentiated to osteoblasts using 300 ng/ml BMP-2 (eBioscience), 10 mM β-glycerophosphate and 50 µg/ml ascorbic acid (Sigma) for 8 days. Calcium phosphate and alkaline phosphatase staining was performed using specific reagents (Alizarin Red S (Sigma) and the BCIP/NBT kit (US Biologicals)).

### *Isolation, FACS, culturing, and differentiation of primary cells*

Isolation and maintenance of sqWAT-derived MSCs was performed as described elsewhere (53). In short, male C57Bl/6J mice aged 8-12 weeks were sacrificed and sqWAT isolated. The tissue was cut into small pieces, digested with collagenase, type II (Sigma), and filtered through a 70 µm mesh to obtain sqWAT MSCs. Freshly isolated cells were seeded on 6 well plates and maintained in DMEM with 10% FBS, 1% Pen/Strep (all ThermoFisher), and 10 mM HEPES. Cells were cultivated for at least 2 passages before inducing differentiation. MSC identity was analyzed by FACS. For differentiation, cells were seeded in 24 or 48 well plates and grown to ~80% confluency. Osteoblastogenesis was induced by 10 mM ß-glycerophosphate, 50 µg/ml ascorbic acid and 50 ng/ml BMP-2 and culture medium changed every other day. Bone-derived MSCs were isolated as previously described (29). In brief, soft-tissue free bones (tibia/femur) were crushed and digested by collagenase, type II (CellSystems) for 1 hour at 37° C and constant agitation. The digest was stopped by adding sorting buffer (2% FBS/PBS). The suspension was filtered through a 70 µm mesh, centrifuged, and the pellet re-suspended in Ammonium-Chloride-Potassium lysis buffer to eliminate red blood cells. After an additional wash step, cells were re-suspended in sorting buffer and antibody-labeled (Table S4). Flow cytometry and cell sorting was conducted on a FACS Aria III cell sorter (BD Biosciences) and analyzed using FlowJo software (Tree Star). Living cells were gated for lack of PI fluorescence and staining of calcein (Sigma). Compensation, fluorescence-minus-one control based gating, and FACS-isolation were conducted as before (54). Freshly isolated cells were maintained and differentiated to adipocytes or osteoblasts as previously (29). Lipid accumulation was determined by Oil Red O staining (Sigma) and calcium deposition by 2% Alizarin Red S staining (Carl Roth). Mouse embryonic fibroblasts were isolated by removing head, limbs, and liver of E13.5 embryos. The remaining tissue was minced and homogenized using a 18 G syringe and seeded in culture flasks. Fibroblasts were grown and expanded in AlphaMEM (Sigma) supplemented with 10% FBS, 1% Pen/Strep.

*Retro and adenoviral infections*

The coding sequences of murine GATA2 sequence was cloned downstream of a Kozak consensus into a retroviral pMSCV vector containing a puromycin resistance cassette (Takara Clontech) and verified by sequencing. EcoPack 2-293 cells (Takara Clontech) were transfected with GATA2 or empty pMSCV vectors using Lipofectamine 2000 (ThermoFisher). The retroviral particles-containing media was harvested 48 hours later. The supernatants were supplemented with 10 µg/ml polybrene and used to infect pre-confluent C3H10T1/2 or primary sqWAT-derived MSCs for 24 hours. 48 hours later, cells were cultured in the presence of 1 µg/ml puromycin. Adenoviruses expressing GFP or Cre were prepared as described previously (55, 56) and equal titers (infectious units (ifu)) used to infect MSCs (1.25E8 ifu/ml in Fig. 7F) or MEFs (3.2E6 ifu/ml) overnight.

*Transfections and luciferase reporter assays*

C3H10T1/2 cells were transfected with pGL4.49 [*luc2P*/TCF-LEF RE] (Promega) or pGL3-*Id1*-BRE (57) vectors by Lipofectamine 2000 (ThermoFisher). 16-20 hours later, cells were stimulated with LiCl (32 mM) or BMP-2 (300 ng/ml) for an additional 4-8 hours and luciferase activity determined. Firefly activity was normalized to co-expressed renilla luciferase (Dual Luciferase Reporter Assay, Promega).

*Chromatin immunoprecipitation (ChIP)*

ChIP analyses in 3T3-L1 and C3H10T1/2 cells were performed as described previously (56). Approx. 100 µg of sonicated chromatin extracts were used for each IP and incubated with 10 µg of a GATA2 antibody (sc-9008x, Santa Cruz) overnight. qPCRs were normalized to the amplification of a fragment of the *insulin* or *36B4* gene. Primers for ChIP-qPCR are listed in Table S5.

*ChIP-seq and analyses*

Pooled DNA from three independent GATA2 ChIPs was used to generate libraries for deep sequencing on Illumina HiSeq instrument. High quality reads were removed if aligning to simple repeat regions and reads were mapped to the mm10 mouse genome assembly. Peaks of 2 independent experiments were called using the MACS2 algorithm (58) with a minimum cutoff of 1% FDR and combined. Called peaks overlapping with ENCODE blacklisted regions for mm10 (59) were removed, as well as peaks located in chr10: 106613366-107858706, chr10: 116174799-118176364 or chrX: 143482886-143483277, since these regions are amplified in 3T3-L1 cells. PhastCons-based average conservation profiles across peak regions (3000 nt around peak center) were computed with the conservation_plot.py script from Tao Liu's open source libraries for bioinformatics (60). Peaks were mapped to neighboring genes within +/- 70 kb using Bedtools windowBed function (61). Genome-wide localization of enriched peak regions were determined using CEAS package (62). Motif search was conducted using SeqPos (14). Gene ontology analysis of genes near GATA2 binding site was performed using DAVID (63, 64). A previously published GATA2 ChIP-seq dataset from murine hematopoietic progenitor cells (20) was analyzed accordingly. Overlapping peaks were identified using intersectBed from Bedtools (65). DeepTools (66) was used to generate heatmaps and signal profiles of peak regions (center ±2 kb). H3K4me1 and H3K27ac ChIP-seq data were obtained from (67) GEO: GSE95533. DNase-seq data were obtained from (68), GEO: GSE27826.

*Blood analysis*

Complete blood cell counts were performed with peripheral blood samples obtained by facial vein or heart puncture from 6-9 months old male mice, immediately stored in tubes containing K3-EDTA anticoagulant (Sarstedt) and analyzed on a XS-800i haematology analyser

(Sysmex) on the same day. A Grubbs' test based outlier analysis was performed using online outlier calculator software (Graphpad Prism), and values with a significance level $\alpha<0.05$ were excluded.

*Protein isolation and immunoblotting*

Cellular proteins were isolated in RIPA buffer and separated by SDS page. After incubation with primary antibodies for GATA2 (sc-9008, Santa Cruz or #4595, Cell Signaling), ZFPM1 (sc-9361, Santa Cruz), or RAN (BD Biosciences) a secondary horseradish-conjugated antibody was added, and a chemiluminescent substrate kit (Roche) was used for detection.

*Isolation of RNA and qantitative PCR (qPCR)*

RNA was purified using spin column kits (Qiagen or Macherey-Nagel). cDNA was generated using the Sprint Powerscript System (Clontech) or MMLV-RT (Promega). qPCR was carried out by using Sybrgreen PCR Mastermix (Eurogentec) and evaluated according to the standard curve method. All RNA expression data were normalized to 36B4 (RPLP0).

*Affymetrix Microarray and heatmaps*

Affymetrix microarray analysis (Mouse Gene 1.1ST, GeneTitan system) and statistical evaluation was performed at the Nutrigenomics technology platform of the University of Wageningen. Row-normalized heatmaps were generated by the Heatmap Builder (69).

*Whole mount embryo staining and histology*

Staining was performed according to a published method (70) with minor modification. Pregnant females were sacrificed at E18.5. Embryos were skinned and eviscerated, fixed in 100% EtOH for 6 hours, stained in 150 mg/l Alcian blue 8 GX (Sigma) for up to 20 hours and incubated in 100% EtOH overnight. Initial clearing was conducted by incubating the embryos

in 2% KOH for 6 hours. Follow-up staining of calcified tissue was done in 50 mg/l Alizarin Red S (Sigma) in 2% KOH for 3 hours. Embryos were sequentially cleared in 2%-0.2% KOH and stored in 100% glycerol. For histology, limbs from 10-12 weeks or 6 months old mice were fixed in 4% PFA, decalcified with Osteosoft (Merck) and paraffinized. 1.5-3 µm sections were stained with Alcian blue 8GX and nuclear fast red (Sigma) as counterstain for growth plate analysis, or with Naphtol AS-MX phosphate (Sigma) and haemalum as counterstain for tartrate-resistant acid phosphatase (TRAP). Osteoclast numbers were quantified by counting multinucleated (n≥3), TRAP-positive cells in the proximal tibia using a Keyence BZ-9000 microscope and ImageJ software. Growth plate height analysis was performed by calculating the mean height from 100 randomly assigned perpendicular distances between the resting and hypertrophic cartilage zones across the complete growth plate in ImageJ.

*Bone metabolic rate analysis*

For dynamic histomorphometry analysis, 10 weeks old male *Gata2* (fl/fl) *Prx1*-Cre negative/positive mice were injected intraperitoneally with 30 µg calcein/g mouse at two time points (9 and 2 days before sacrificing). Tibiae were collected, cleared of soft tissue and fixed in 4% PFA for two days. Samples were washed and dehydrated gradually in 70%, 80%, 90% to 100% EtOH during a period of 12 days. Technovit 9100 system (Kulzer) was used for infiltration and polymerization. Calcein double labelling was captured with the Keyence BZ-9000 fluorescence microscope and analyzed by an ImageJ macro (71). Exclusion criteria were predefined as lack of two distinguishable fluorescent calcein labels. Mineral apposition rate (MAR) was calculated according to international standards (72).

*Bone µCT and analyses*

Bone µCT analysis was adapted from our previously used method (73). Dissected hind limbs of 10-12 weeks old male or 8 months old male mice were pruned of soft tissue and scanned on a VivaCT 40 platform (SCANCO Medical AG) using a voxel size of 10.5 µm, $E$=70 kV, $I$=114 µA and an integration time of 381 ms. Histomorphometric analysis for metaphysis, proximal, and mid-diaphysis regions was performed using SCANCO Medical software and the BoneJ-plugin (74) for ImageJ software.

*Biomechanical bone testing*

Biomechanical whole bone strength was studied in femora from 10-12 weeks and 6 months old male mice in destructive three-point bending experiments using a LM 1 ElectroForce Test Bench (Bose). Explanted femora were mounted anterior side up for bending tests at a 8.5 mm span width between the end supports. The load was applied to the anterior midshaft of the femur at a constant deflection rate of 0.1 mm/s. Load (50 lbs / 225 N load cell) and displacement data were sampled at 100 Hz. Stiffness, maximum load, load to failure and deflection at failure at fracture were calculated from the force-deflection curve using a routine written in MATLAB (The Mathworks, Inc.).

*Bone fracture healing model*

The fracture healing model was performed as described previously (29). Briefly, eight months old male mice were given an analgetic (MediGel, ClearH2O) starting two days prior to surgery. At the day of surgery mice were anesthetized and a steel pin (diameter 0.35 mm) was inserted into the medullary cavity through a small cutaneous incision at the knee joint for stabilization followed by a fracture induction with scissors 0.5 cm distal from the knee. 14 days after fracture induction, tibiae were harvested for analyses. After removal of the pin, the extracted tibiae were fixed and a µCT analysis was conducted. Subsequently, tibiae were decalcified followed by paraffin embedding and sectioning at 3 mm per slice. Samples were

stained using SafraninO/Fast green and Movat Pentachrome. ImageJ software was used for computer-assisted histomorphometric analysis of fracture calluses. Six representative sections of each callus were analyzed for bone, fibrous and cartilaginous tissue areas in a blinded manner.

*Data accessibility*

GATA2 ChIP-seq data for 3T3-L1 and C3H10T1/2 cells and Affymetrix microarray data of primary cells over-expressing GATA2 are available at the GEO database under the accession code GSE101592.

*Statistical analysis*

Significance was determined by the 2-tailed Student's *t* test or ANOVA, as appropriate, and $P < 0.05$ was deemed significant ($*P < 0.05$). Representative results of at least three independent cell culture experiments are shown and presented as mean ± s.d. Mouse data are presented as mean ± s.e.m.

**ACKNOWLEDGEMENTS**

This work was supported by the Einstein Foundation Berlin (grant nr. A-2011-83) to M. S. and S. S, by the Career Integration Grant from the European Commission (CIG 291867), the German Research Foundation (DFG, Emmy Noether grant SCHU 2546/1-1), and by the 'Deutsche Diabetes Stiftung' (grant nr. 280-12-10) to M.S., and by a DynAge Focus Area grant to M. S. and T. J. S. We thank Dr. Mathias Treier (Max-Delbrück Center, Berlin Buch) for sharing Prx1-Cre mice and Dr. Christian Freise (Charité) for sharing WNT reporter constructs. pGL3 BRE Luciferase was a gift from Martine Roussel & Peter ten Dijke (Addgene plasmid # 45126). We thank Dr. Jan Tuckermann and colleagues (University of Ulm) for methodological help on bone characterization. This study was initiated in the

laboratory of Dr. Mitch Lazar (Perelman School of Medicine, University of Pennsylvania, Philadelphia) and we are deeply grateful for his support. A.T. and M.S. conceived and designed experiments. A.T., C.F., T.H.A., M. B., C.T.H., M.M., S.M., M.T., S.H. M., S.S., T.J.S. and M.S. performed experiments and/or analyzed data. M.Sa. provided a genetic mouse model and G.S. assisted with blood analyses. G.N.D. assisted with bone characterization. A.T., C.F., T.H.A, S. H. M., S.S, T.J.S., and M.S. wrote and edited the manuscript.

## REFERENCES

1. **Tsai, F. Y., G. Keller, F. C. Kuo, M. Weiss, J. Chen, M. Rosenblatt, F. W. Alt, and S. H. Orkin.** 1994. An early haematopoietic defect in mice lacking the transcription factor GATA-2. Nature **371:**221-6.

2. **Tsai, F. Y., and S. H. Orkin.** 1997. Transcription factor GATA-2 is required for proliferation/survival of early hematopoietic cells and mast cell formation, but not for erythroid and myeloid terminal differentiation. Blood **89:**3636-43.

3. **Spinner, M. A., L. A. Sanchez, A. P. Hsu, P. A. Shaw, C. S. Zerbe, K. R. Calvo, D. C. Arthur, W. Gu, C. M. Gould, C. C. Brewer, E. W. Cowen, A. F. Freeman, K. N. Olivier, G. Uzel, A. M. Zelazny, J. R. Daub, C. D. Spalding, R. J. Claypool, N. K. Giri, B. P. Alter, E. M. Mace, J. S. Orange, J. Cuellar-Rodriguez, D. D. Hickstein, and S. M. Holland.** 2014. GATA2 deficiency: a protean disorder of hematopoiesis, lymphatics, and immunity. Blood **123:**809-21.

4. **Crispino, J. D., and M. S. Horwitz.** 2017. GATA factor mutations in hematologic disease. Blood **129:**2103-2110.

5. **Kamata, M., Y. Okitsu, T. Fujiwara, M. Kanehira, S. Nakajima, T. Takahashi, A. Inoue, N. Fukuhara, Y. Onishi, K. Ishizawa, R. Shimizu, M. Yamamoto, and H. Harigae.** 2014. GATA2 regulates differentiation of bone marrow-derived mesenchymal stem cells. Haematologica **99:**1686-96.

6. **Tong, Q., G. Dalgin, H. Xu, C. N. Ting, J. M. Leiden, and G. S. Hotamisligil.** 2000. Function of GATA transcription factors in preadipocyte-adipocyte transition. Science **290:**134-8.

7. **Tsai, J., Q. Tong, G. Tan, A. N. Chang, S. H. Orkin, and G. S. Hotamisligil.** 2005. The transcription factor GATA2 regulates differentiation of brown adipocytes. EMBO Rep **6:**879-84.

8. **Tong, Q., J. Tsai, G. Tan, G. Dalgin, and G. S. Hotamisligil.** 2005. Interaction between GATA and the C/EBP family of transcription factors is critical in GATA-mediated suppression of adipocyte differentiation. Mol Cell Biol **25:**706-15.

9. **Cantor, A. B., and S. H. Orkin.** 2005. Coregulation of GATA factors by the Friend of GATA (FOG) family of multitype zinc finger proteins. Semin Cell Dev Biol **16:**117-28.

10. **Welch, J. J., J. A. Watts, C. R. Vakoc, Y. Yao, H. Wang, R. C. Hardison, G. A. Blobel, L. A. Chodosh, and M. J. Weiss.** 2004. Global regulation of erythroid gene expression by transcription factor GATA-1. Blood **104:**3136-47.

11. **Green, H., and M. Meuth.** 1974. An established pre-adipose cell line and its differentiation in culture. Cell **3:**127-33.

12. **Schupp, M., A. G. Cristancho, M. I. Lefterova, E. A. Hanniman, E. R. Briggs, D. J. Steger, M. Qatanani, J. C. Curtin, J. Schug, S. A. Ochsner, N. J. McKenna, and M. A. Lazar.** 2009. Re-expression of GATA2 Cooperates with Peroxisome Proliferator-activated Receptor-{gamma} Depletion to Revert the Adipocyte Phenotype. J Biol Chem **284:**9458-64.

13. **Jack, B. H., and M. Crossley.** 2010. GATA proteins work together with friend of GATA (FOG) and C-terminal binding protein (CTBP) co-regulators to control adipogenesis. J Biol Chem **285:**32405-14.

14. **He, H. H., C. A. Meyer, H. Shin, S. T. Bailey, G. Wei, Q. Wang, Y. Zhang, K. Xu, M. Ni, M. Lupien, P. Mieczkowski, J. D. Lieb, K. Zhao, M. Brown, and X. S. Liu.** 2010. Nucleosome dynamics define transcriptional enhancers. Nat Genet **42:**343-7.

15. **Martin, D. I., and S. H. Orkin.** 1990. Transcriptional activation and DNA binding by the erythroid factor GF-1/NF-E1/Eryf 1. Genes Dev **4:**1886-98.

16. **Fujiwara, T., H. O'Geen, S. Keles, K. Blahnik, A. K. Linnemann, Y. A. Kang, K. Choi, P. J. Farnham, and E. H. Bresnick.** 2009. Discovering hematopoietic mechanisms through genome-wide analysis of GATA factor chromatin occupancy. Mol Cell **36:**667-81.

17. **Evans, T., M. Reitman, and G. Felsenfeld.** 1988. An erythrocyte-specific DNA-binding factor recognizes a regulatory sequence common to all chicken globin genes. Proc Natl Acad Sci U S A **85:**5976-80.

18. **Wadman, I. A., H. Osada, G. G. Grutz, A. D. Agulnick, H. Westphal, A. Forster, and T. H. Rabbitts.** 1997. The LIM-only protein Lmo2 is a bridging molecule assembling an erythroid, DNA-binding complex which includes the TAL1, E47, GATA-1 and Ldb1/NLI proteins. EMBO J **16:**3145-57.

19. **Siepel, A., G. Bejerano, J. S. Pedersen, A. S. Hinrichs, M. Hou, K. Rosenbloom, H. Clawson, J. Spieth, L. W. Hillier, S. Richards, G. M. Weinstock, R. K. Wilson, R. A. Gibbs, W. J. Kent, W. Miller, and D. Haussler.** 2005. Evolutionarily conserved elements in vertebrate, insect, worm, and yeast genomes. Genome Res **15:**1034-50.

20. **May, G., S. Soneji, A. J. Tipping, J. Teles, S. J. McGowan, M. Wu, Y. Guo, C. Fugazza, J. Brown, G. Karlsson, C. Pina, V. Olariu, S. Taylor, D. G. Tenen, C. Peterson, and T. Enver.** 2013. Dynamic analysis of gene expression and genome-wide transcription factor binding during lineage specification of multipotent progenitors. Cell Stem Cell **13:**754-68.

21. **Spooncer, E., C. M. Heyworth, A. Dunn, and T. M. Dexter.** 1986. Self-renewal and differentiation of interleukin-3-dependent multipotent stem cells are modulated by stromal cells and serum factors. Differentiation **31:**111-8.

22. **Rux, D. R., and D. M. Wellik.** 2017. Hox genes in the adult skeleton: Novel functions beyond embryonic development. Dev Dyn **246:**310-317.

23. **Kam, M. K., and V. C. Lui.** 2015. Roles of Hoxb5 in the development of vagal and trunk neural crest cells. Dev Growth Differ **57:**158-68.

24. **Reznikoff, C. A., D. W. Brankow, and C. Heidelberger.** 1973. Establishment and characterization of a cloned line of C3H mouse embryo cells sensitive to postconfluence inhibition of division. Cancer Res **33:**3231-8.

25. **Wu, M., G. Chen, and Y. P. Li.** 2016. TGF-beta and BMP signaling in osteoblast, skeletal development, and bone formation, homeostasis and disease. Bone Res **4:**16009.

26. **Karsenty, G.** 2008. Transcriptional control of skeletogenesis. Annu Rev Genomics Hum Genet **9:**183-96.

27. **Haugas, M., K. Lillevali, J. Hakanen, and M. Salminen.** 2010. Gata2 is required for the development of inner ear semicircular ducts and the surrounding perilymphatic space. Dev Dyn **239:**2452-69.

28. **Logan, M., J. F. Martin, A. Nagy, C. Lobe, E. N. Olson, and C. J. Tabin.** 2002. Expression of Cre Recombinase in the developing mouse limb bud driven by a Prxl enhancer. Genesis **33:**77-80.

29. **Ambrosi, T. H., A. Scialdone, A. Graja, S. Gohlke, A. M. Jank, C. Bocian, L. Woelk, H. Fan, D. W. Logan, A. Schurmann, L. R. Saraiva, and T. J. Schulz.** 2017. Adipocyte Accumulation in the Bone Marrow during Obesity and Aging Impairs Stem Cell-Based Hematopoietic and Bone Regeneration. Cell Stem Cell **20:**771-784 e6.

30. **Sanchez-Gurmaches, J., W. Y. Hsiao, and D. A. Guertin.** 2015. Highly selective in vivo labeling of subcutaneous white adipocyte precursors with Prx1-Cre. Stem Cell Reports **4:**541-50.

31. **Krueger, K. C., M. J. Costa, H. Du, and B. J. Feldman.** 2014. Characterization of Cre recombinase activity for in vivo targeting of adipocyte precursor cells. Stem Cell Reports **3:**1147-58.

32. **Yasuda, H., N. Shima, N. Nakagawa, K. Yamaguchi, M. Kinosaki, S. Mochizuki, A. Tomoyasu, K. Yano, M. Goto, A. Murakami, E. Tsuda, T. Morinaga, K. Higashio, N. Udagawa, N. Takahashi, and T. Suda.** 1998. Osteoclast differentiation factor is a ligand for osteoprotegerin/osteoclastogenesis-inhibitory factor and is identical to TRANCE/RANKL. Proc Natl Acad Sci U S A **95:**3597-602.

33. **Kong, Y. Y., H. Yoshida, I. Sarosi, H. L. Tan, E. Timms, C. Capparelli, S. Morony, A. J. Oliveira-dos-Santos, G. Van, A. Itie, W. Khoo, A. Wakeham, C. R. Dunstan, D. L. Lacey, T. W. Mak, W. J. Boyle, and J. M. Penninger.** 1999. OPGL is a key regulator of osteoclastogenesis, lymphocyte development and lymph-node organogenesis. Nature **397:**315-23.

34. **Takahashi, N., N. Udagawa, T. Akatsu, H. Tanaka, M. Shionome, and T. Suda.** 1991. Role of colony-stimulating factors in osteoclast development. J Bone Miner Res **6:**977-85.

35. **Simonet, W. S., D. L. Lacey, C. R. Dunstan, M. Kelley, M. S. Chang, R. Luthy, H. Q. Nguyen, S. Wooden, L. Bennett, T. Boone, G. Shimamoto, M. DeRose, R. Elliott, A. Colombero, H. L. Tan, G. Trail, J. Sullivan, E. Davy, N. Bucay, L. Renshaw-Gegg, T. M. Hughes, D. Hill, W. Pattison, P. Campbell, S. Sander, G. Van, J. Tarpley, P. Derby, R. Lee, and W. J. Boyle.** 1997. Osteoprotegerin: a novel secreted protein involved in the regulation of bone density. Cell **89:**309-19.

687 36. **Wada, T., T. Nakashima, N. Hiroshi, and J. M. Penninger.** 2006. RANKL-RANK
688 signaling in osteoclastogenesis and bone disease. Trends Mol Med **12:**17-25.
689 37. **Horowitz, M. C., Y. Xi, K. Wilson, and M. A. Kacena.** 2001. Control of
690 osteoclastogenesis and bone resorption by members of the TNF family of receptors
691 and ligands. Cytokine Growth Factor Rev **12:**9-18.
692 38. **Liu, Z., D. Merkurjev, F. Yang, W. Li, S. Oh, M. J. Friedman, X. Song, F. Zhang,**
693 **Q. Ma, K. A. Ohgi, A. Krones, and M. G. Rosenfeld.** 2014. Enhancer activation
694 requires trans-recruitment of a mega transcription factor complex. Cell **159:**358-73.
695 39. **Bucay, N., I. Sarosi, C. R. Dunstan, S. Morony, J. Tarpley, C. Capparelli, S.**
696 **Scully, H. L. Tan, W. Xu, D. L. Lacey, W. J. Boyle, and W. S. Simonet.** 1998.
697 osteoprotegerin-deficient mice develop early onset osteoporosis and arterial
698 calcification. Genes Dev **12:**1260-8.
699 40. **Meijome, T. E., R. A. Hooker, Y. H. Cheng, W. Walker, M. C. Horowitz, R. K.**
700 **Fuchs, and M. A. Kacena.** 2015. GATA-1 deficiency rescues trabecular but not
701 cortical bone in OPG deficient mice. J Cell Physiol **230:**783-90.
702 41. **Yamane, T., T. Kunisada, H. Yamazaki, T. Nakano, S. H. Orkin, and S. I.**
703 **Hayashi.** 2000. Sequential requirements for SCL/tal-1, GATA-2, macrophage colony-
704 stimulating factor, and osteoclast differentiation factor/osteoprotegerin ligand in
705 osteoclast development. Exp Hematol **28:**833-40.
706 42. **Wei, W., D. Zeve, X. Wang, Y. Du, W. Tang, P. C. Dechow, J. M. Graff, and Y.**
707 **Wan.** 2011. Osteoclast progenitors reside in the peroxisome proliferator-activated
708 receptor gamma-expressing bone marrow cell population. Mol Cell Biol **31:**4692-705.
709 43. **Wei, W., D. Zeve, J. M. Suh, X. Wang, Y. Du, J. E. Zerwekh, P. C. Dechow, J. M.**
710 **Graff, and Y. Wan.** 2011. Biphasic and dosage-dependent regulation of
711 osteoclastogenesis by beta-catenin. Mol Cell Biol **31:**4706-19.

44. **Kao, S. Y., J. S. Kempfle, J. B. Jensen, D. Perez-Fernandez, A. C. Lysaght, A. S. Edge, and K. M. Stankovic.** 2013. Loss of osteoprotegerin expression in the inner ear causes degeneration of the cochlear nerve and sensorineural hearing loss. Neurobiol Dis **56:**25-33.

45. **Grasemann, C., N. Unger, M. Hovel, D. Arweiler-Harbeck, R. Herrmann, M. M. Schundeln, O. Muller, B. Schweiger, E. Lausch, T. Meissner, C. Kiewert, B. P. Hauffa, and N. J. Shaw.** 2017. Loss of Functional Osteoprotegerin: More Than a Skeletal Problem. J Clin Endocrinol Metab **102:**210-219.

46. **Li, X., H. Huynh, H. Zuo, M. Salminen, and Y. Wan.** 2016. Gata2 Is a Rheostat for Mesenchymal Stem Cell Fate in Male Mice. Endocrinology **157:**1021-8.

47. **Hasegawa, S., T. Fujiwara, Y. Okitsu, H. Kato, Y. Sato, N. Fukuhara, Y. Onishi, R. Shimizu, M. Yamamoto, and H. Harigae.** 2017. Effects of in vivo deletion of GATA2 in bone marrow stromal cells. Exp Hematol.

48. **Boulais, P. E., and P. S. Frenette.** 2015. Making sense of hematopoietic stem cell niches. Blood **125:**2621-9.

49. **Kacena, M. A., C. M. Gundberg, and M. C. Horowitz.** 2006. A reciprocal regulatory interaction between megakaryocytes, bone cells, and hematopoietic stem cells. Bone **39:**978-84.

50. **Miyamoto, K., S. Yoshida, M. Kawasumi, K. Hashimoto, T. Kimura, Y. Sato, T. Kobayashi, Y. Miyauchi, H. Hoshi, R. Iwasaki, H. Miyamoto, W. Hao, H. Morioka, K. Chiba, H. Yasuda, J. M. Penninger, Y. Toyama, T. Suda, and T. Miyamoto.** 2011. Osteoclasts are dispensable for hematopoietic stem cell maintenance and mobilization. J Exp Med **208:**2175-81.

51. **Schweikle, E., T. Baessler, S. Yildirim, L. Kanz, R. Mohle, and K. C. Weisel.** 2012. Osteoprotegerin positively regulates hematopoietic progenitor cells. Curr Stem Cell Res Ther **7:**72-7.

738 52. **Witte, N., M. Muenzner, J. Rietscher, M. Knauer, S. Heidenreich, A. M. Nuotio-**
739 **Antar, F. A. Graef, R. Fedders, A. Tolkachov, I. Goehring, and M. Schupp.** 2015.
740 The Glucose Sensor ChREBP Links De Novo Lipogenesis to PPARgamma Activity
741 and Adipocyte Differentiation. Endocrinology **156:**4008-19.
742 53. **Siersbaek, M. S., A. Loft, M. M. Aagaard, R. Nielsen, S. F. Schmidt, N. Petrovic,**
743 **J. Nedergaard, and S. Mandrup.** 2012. Genome-wide profiling of peroxisome
744 proliferator-activated receptor gamma in primary epididymal, inguinal, and brown
745 adipocytes reveals depot-selective binding correlated with gene expression. Mol Cell
746 Biol **32:**3452-63.
747 54. **Schulz, T. J., T. L. Huang, T. T. Tran, H. Zhang, K. L. Townsend, J. L.**
748 **Shadrach, M. Cerletti, L. E. McDougall, N. Giorgadze, T. Tchkonia, D. Schrier,**
749 **D. Falb, J. L. Kirkland, A. J. Wagers, and Y. H. Tseng.** 2011. Identification of
750 inducible brown adipocyte progenitors residing in skeletal muscle and white fat. Proc
751 Natl Acad Sci U S A **108:**143-8.
752 55. **Muenzner, M., N. Tuvia, C. Deutschmann, N. Witte, A. Tolkachov, A. Valai, A.**
753 **Henze, L. E. Sander, J. Raila, and M. Schupp.** 2013. Retinol-binding protein 4 and
754 its membrane receptor STRA6 control adipogenesis by regulating cellular retinoid
755 homeostasis and retinoic acid receptor alpha activity. Mol Cell Biol **33:**4068-82.
756 56. **Schupp, M., M. I. Lefterova, J. Janke, K. Leitner, A. G. Cristancho, S. E.**
757 **Mullican, M. Qatanani, N. Szwergold, D. J. Steger, J. C. Curtin, R. J. Kim, M.**
758 **Suh, M. R. Albert, S. Engeli, L. J. Gudas, and M. A. Lazar.** 2009. Retinol saturase
759 promotes adipogenesis and is downregulated in obesity. Proc Natl Acad Sci U S A
760 **106:**1105-10.
761 57. **Korchynskyi, O., and P. ten Dijke.** 2002. Identification and functional
762 characterization of distinct critically important bone morphogenetic protein-specific
763 response elements in the Id1 promoter. J Biol Chem **277:**4883-91.

764 58. **Zhang, Y., T. Liu, C. A. Meyer, J. Eeckhoute, D. S. Johnson, B. E. Bernstein, C.**
765 **Nusbaum, R. M. Myers, M. Brown, W. Li, and X. S. Liu.** 2008. Model-based
766 analysis of ChIP-Seq (MACS). Genome Biol **9:**R137.
767 59. **Consortium, E. P.** 2012. An integrated encyclopedia of DNA elements in the human
768 genome. Nature **489:**57-74.
769 60. **Shin, H., T. Liu, X. Duan, Y. Zhang, and X. S. Liu.** 2013. Computational
770 methodology for ChIP-seq analysis. Quant Biol **1:**54-70.
771 61. **Quinlan, A. R., and I. M. Hall.** 2010. BEDTools: a flexible suite of utilities for
772 comparing genomic features. Bioinformatics **26:**841-2.
773 62. **Shin, H., T. Liu, A. K. Manrai, and X. S. Liu.** 2009. CEAS: cis-regulatory element
774 annotation system. Bioinformatics **25:**2605-6.
775 63. **Huang da, W., B. T. Sherman, and R. A. Lempicki.** 2009. Systematic and
776 integrative analysis of large gene lists using DAVID bioinformatics resources. Nat
777 Protoc **4:**44-57.
778 64. **Huang da, W., B. T. Sherman, and R. A. Lempicki.** 2009. Bioinformatics
779 enrichment tools: paths toward the comprehensive functional analysis of large gene
780 lists. Nucleic Acids Res **37:**1-13.
781 65. **Quinlan, A. R.** 2014. BEDTools: The Swiss-Army Tool for Genome Feature
782 Analysis. Curr Protoc Bioinformatics **47:**11 12 1-34.
783 66. **Ramirez, F., F. Dundar, S. Diehl, B. A. Gruning, and T. Manke.** 2014. deepTools:
784 a flexible platform for exploring deep-sequencing data. Nucleic Acids Res **42:**W187-
785 91.
786 67. **Siersbaek, R., J. G. S. Madsen, B. M. Javierre, R. Nielsen, E. K. Bagge, J. Cairns,**
787 **S. W. Wingett, S. Traynor, M. Spivakov, P. Fraser, and S. Mandrup.** 2017.
788 Dynamic Rewiring of Promoter-Anchored Chromatin Loops during Adipocyte
789 Differentiation. Mol Cell **66:**420-435 e5.

68. **Siersbaek, R., R. Nielsen, S. John, M. H. Sung, S. Baek, A. Loft, G. L. Hager, and S. Mandrup.** 2011. Extensive chromatin remodelling and establishment of transcription factor 'hotspots' during early adipogenesis. EMBO J **30:**1459-72.

69. **King, J. Y., R. Ferrara, R. Tabibiazar, J. M. Spin, M. M. Chen, A. Kuchinsky, A. Vailaya, R. Kincaid, A. Tsalenko, D. X. Deng, A. Connolly, P. Zhang, E. Yang, C. Watt, Z. Yakhini, A. Ben-Dor, A. Adler, L. Bruhn, P. Tsao, T. Quertermous, and E. A. Ashley.** 2005. Pathway analysis of coronary atherosclerosis. Physiol Genomics **23:**103-18.

70. **Mallo, M., and I. Brandlin.** 1997. Segmental identity can change independently in the hindbrain and rhombencephalic neural crest. Dev Dyn **210:**146-56.

71. **Schindelin, J., I. Arganda-Carreras, E. Frise, V. Kaynig, M. Longair, T. Pietzsch, S. Preibisch, C. Rueden, S. Saalfeld, B. Schmid, J. Y. Tinevez, D. J. White, V. Hartenstein, K. Eliceiri, P. Tomancak, and A. Cardona.** 2012. Fiji: an open-source platform for biological-image analysis. Nat Methods **9:**676-82.

72. **Dempster, D. W., J. E. Compston, M. K. Drezner, F. H. Glorieux, J. A. Kanis, H. Malluche, P. J. Meunier, S. M. Ott, R. R. Recker, and A. M. Parfitt.** 2013. Standardized nomenclature, symbols, and units for bone histomorphometry: a 2012 update of the report of the ASBMR Histomorphometry Nomenclature Committee. J Bone Miner Res **28:**2-17.

73. **Willie, B. M., A. I. Birkhold, H. Razi, T. Thiele, M. Aido, B. Kruck, A. Schill, S. Checa, R. P. Main, and G. N. Duda.** 2013. Diminished response to in vivo mechanical loading in trabecular and not cortical bone in adulthood of female C57Bl/6 mice coincides with a reduction in deformation to load. Bone **55:**335-46.

74. **Doube, M., M. M. Klosowski, I. Arganda-Carreras, F. P. Cordelieres, R. P. Dougherty, J. S. Jackson, B. Schmid, J. R. Hutchinson, and S. J. Shefelbine.** 2010. BoneJ: Free and extensible bone image analysis in ImageJ. Bone **47:**1076-9.

816

817 **FIGURE LEGENDS**

818

819 **Fig. 1** GATA2 binds at canonical WGATAR-motifs in the genome of 3T3-L1 cells and is
820 enriched near genes involved in skeletal development. (*A*) GATA2 protein expression in 3T3-
821 L1 preadipocytes (Day 0) and adipocytes (Day 14 after the initiation of differentiation)
822 determined by immunoblotting. RAN protein served as loading control. (*B*) *Zfpm1* mRNA in
823 3T3-L1 preadipocytes and adipocytes was analyzed by qPCR. (*C*) GATA2 was retrovirally
824 over-expressed in 3T3-L1 cells and protein expression of GATA2 and ZFPM1 determined by
825 immunoblotting. RAN protein served as loading control. (*D*) Chromatin immunoprecipitation
826 (ChIP) of endogenously expressed GATA2 in undifferentiated and differentiated 3T3-L1
827 revealed preadipocyte-specific binding of GATA2 to the *Zfpm1* gene locus (+0.7 kb). (*E*)
828 Genomic localization of the 1,975 GATA2 binding sites in 3T3-L1 cells called by the MACS
829 algorithm. (*F*) Top 3 enriched *de novo* motif clusters identified by SeqPos. (*G*) Identification
830 of E-box motifs in GATA2 bound regions by *de novo* motif analysis with SeqPos (top panel).
831 Top four clusters of known transcription factor motifs enriched in GATA2 binding sites
832 determined by SeqPos (bottom panel). (*H*) PhastCons evaluation of GATA2 binding sites for
833 evolutionary sequence conservation. (*I*) Gene ontology (GO) analysis of nearest genes (±70
834 kb of binding sites, n=2,230 genes) showing the term for 'skeletal system development' (n=56
835 genes, Table S1) genes represented among the top ranked clusters. Data are presented as mean
836 ± s.d. and $*P < 0.05$

837

838 **Fig. 2** Cell type-specific binding of GATA2 in mesenchymal and hematopoietic cells. (*A*)
839 Intersection of nearest genes (±70 kb of binding sites) between mesenchymal 3T3-L1 and
840 hematopoietic FDCPmix (mHSC) cells. (*B*) Average profile of the ChIP-seq signal of the
841 indicated chromatin marks and DNase I hypersensitivity (DHS) in 3T3-L1 preadipocytes

around GATA2 binding sites. (*C*) GO analysis of cell type-specific or overlapping nearest genes from (*A*) showing the top two ranked clusters. The corresponding cell type-specific peaks were analyzed for known transcription factor binding motifs besides the GATA motif (right panel). (*D*) GATA2 binding in C3H10T1/2 cells near *Zfpm1* and *Ccna1* is conserved and ChIP-seq identified 1,517 peaks and WGATAR as the most enriched motif (*de novo*). 51% of nearest genes (±70 kb of binding sites) in C3H10T1/2 cells overlapped with those in 3T3-L1 cells. (*E*) Heatmap visualization of genome wide GATA2 read coverage between 3T3-L1, C3H10T1/2 and FDCPmix cells. In (*D*), data are presented as mean ± s.d. and $*P < 0.05$

**Fig. 3** Ectopic expression of GATA2 in MSCs blocks osteoblast differentiation and interferes with BMP-driven SMAD activation. (*A*) C3H10T1/2 cells were infected with empty-or GATA2-expressing retroviruses and *Gata2* mRNA levels determined by qPCR and then induced to differentiate into osteoblasts. 8 days later, differentiation was assessed by (*B*) alkaline phosphatase (ALPL) staining and calcium precipitation by Alizarin and (*C*) the expression of osteoblast marker genes by qPCR. (*D*) and (*E*) Undifferentiated C3H10T1/2 cells described in (*A*) were transfected with (*D*) SMAD1/5/8-RE or (*E*) TCF/LEF-RE-driven reporter vectors, stimulated with 300 ng/ml BMP2 or 32 mM LiCl as indicated, and luciferase activity determined. (*F*) sqWAT-derived Lin-Sca+ cells were infected as described in (A) and *Gata2* mRNA levels determined. (*G*) Cells described in (*F*) were analyzed by Affymetrix gene expression profiling. Expression of GATA2-bound genes (±70 kb of binding sites) mapped to GO skeletal morphogenesis and development-related pathways (n=102 genes) was visualized by a heatmap. Gene symbols are given for genes up-or down-regulated (n=41, $q < 0.05$). (*H*) Heatmap of selected genes involved in SMAD signaling. Cells were induced to differentiate into osteoblasts. 8 days later, differentiation was assessed by (*I*) ALPL staining and calcium precipitation by Alizarin and (*J*) the expression of osteoblast marker genes by

qPCR. Data are presented as mean ± s.d. and *$P$ < 0.05 of Retro GATA2 vs. Retro empty, (*D* and *E*) #$P$ < 0.05 of BMP2 and LiCl treatment vs. untreated Retro empty.

**Fig.4** MSC-specific deletion of GATA2 in mice increases the number of bone-residing precursor and promotes their osteoblastogenic differentiation *in vitro*. (*A*) Lin- Sca1+ cells from various tissues of mesenchymal origin from Prx1-Cre positive/negative mice with floxed *Gata2* alleles were isolated and analyzed for expression of *Gata2* by qPCR (n=4,4). (*B*) Deletion of GATA2 protein in sqWAT-derived Lin- Sca1+ cells was validated by immunoblotting. (*C*) Lin- Sca1+ cells with or without *Gata2* expression were analyzed for a compensatory up-regulation of other GATA factors by qPCR (n=4,4). (*D*) Relative abundance of adipogenic (Lin- Sca1+) and osteoblastic (Lin- Sca1- Pdgfra+) precursors isolated from bone of Prx1-Cre positive/negative mice with floxed *Gata2* alleles (n=14,11). *(E)* Ostoblastogenesis of Lin- Sca+ cells derived from bone was assessed by Alizarin staining of calcium precipitation and (F) the expression of osteoblast marker genes by qPCR (n=3,3). *(G)* Ostoblastogenesis of Lin- Sca1+ Pdgfra+ cells derived from bone was assessed by Alizarin staining of calcium precipitation and (*H*) the expression of osteoblast marker genes by qPCR (n=3,3). Data are presented as mean ± s.d. (mean ± s.e.m. in *D*) and *$P$ < 0.05 between Cre (+) and Cre (-) cells or mice.

**Fig. 5** MSC-specific deletion of GATA2 impairs trabecular bone structure and bone durability in aged mice. (*A*) E18.5 Prx1-Cre positive/negative embryos with floxed *Gata2* alleles were stained with Alizarin red and Alcian blue to assess mineralization and cartilage pattern (top). Alcian blue staining of longitudinal sections of proximal tibiae growth plates and height quantifications from three months old mice (bottom, n=5,6). (*B*) µCT analyses of 1-metaphysis, 2-proximal, and 3-mid diaphysis of tibiae from three months old mice. (*C*) Histomorphometric analysis of the medulary cavity of proximal diaphysis for bone surface

and trabeculae numbers in three months old mice of the indicated genotypes (n=6,6). (*D*) Three-point-bending of tibiae from three (n=4,4) and six (n=7,4) months old mice of the indicated genotypes. Data are presented as mean ± s.e.m. and **P* < 0.05 between Cre (+) and Cre (-) mice. Scale bars: (*A*, top) 2.5 mm, (*A*, bottom) 100 µm, (*B*, left) 1 mm, (*B*, right) 0.5 mm.

**Fig. 6** MSC-specific deletion of GATA2 affects bone turnover and blood cell counts. (*A*) Assessment of the mineral apposition rate (MAR) by quantification of double calcein-labeled trabecular sections of tibial bones of three month old mice (n=4,5). (*B*) Bone marrow-free femora of six months old mice with floxed *Gata2* alleles and the indicated genotype were analyzed for osteoclast marker gene expression by qPCR (n=3,3). (*C*) Tartrate-resistant acid phosphatase (TRAP) staining and quantification in proximal tibiae of six months old mice of the indicated genotype (n=4,4). (*D*) mRNA expression of *Rankl*, *Csf1*, and *Opg* in the material described in (*B*) were determined by qPCR. (*E*) GATA2 binding near *Tnfrsf11b* (=*Opg*) gene locus in mesenchymal (C3H10T1/2) and hematopoietic cells (FDCPmix) shown in the UCSC Genome Browser. (*F*) ChIP-qPCR validation of GATA2 binding upstream (-13.0 and -75.4 kb) of the *Opg* TSS in C3H10T1/2 cells. (*G*) Bone-derived Lin- Sca1+ precursor cells, isolated from mice with floxed *Gata2* alleles, were infected with GFP or Cre-expressing adenoviruses. *Opg* mRNA expression was determined 96 hours later by qPCR. (*H*) Blood cell analysis of six-nine months old Prx1-Cre positive/negative mice with floxed *Gata2* alleles (n=25,20). In (*A-D*), data are presented as mean ± s.e.m., in (*F*) and (*G*) data are presented as mean ± s.d., and **P* < 0.05. Scale bars (*A*): 25 µm, (*C*): 50 µM

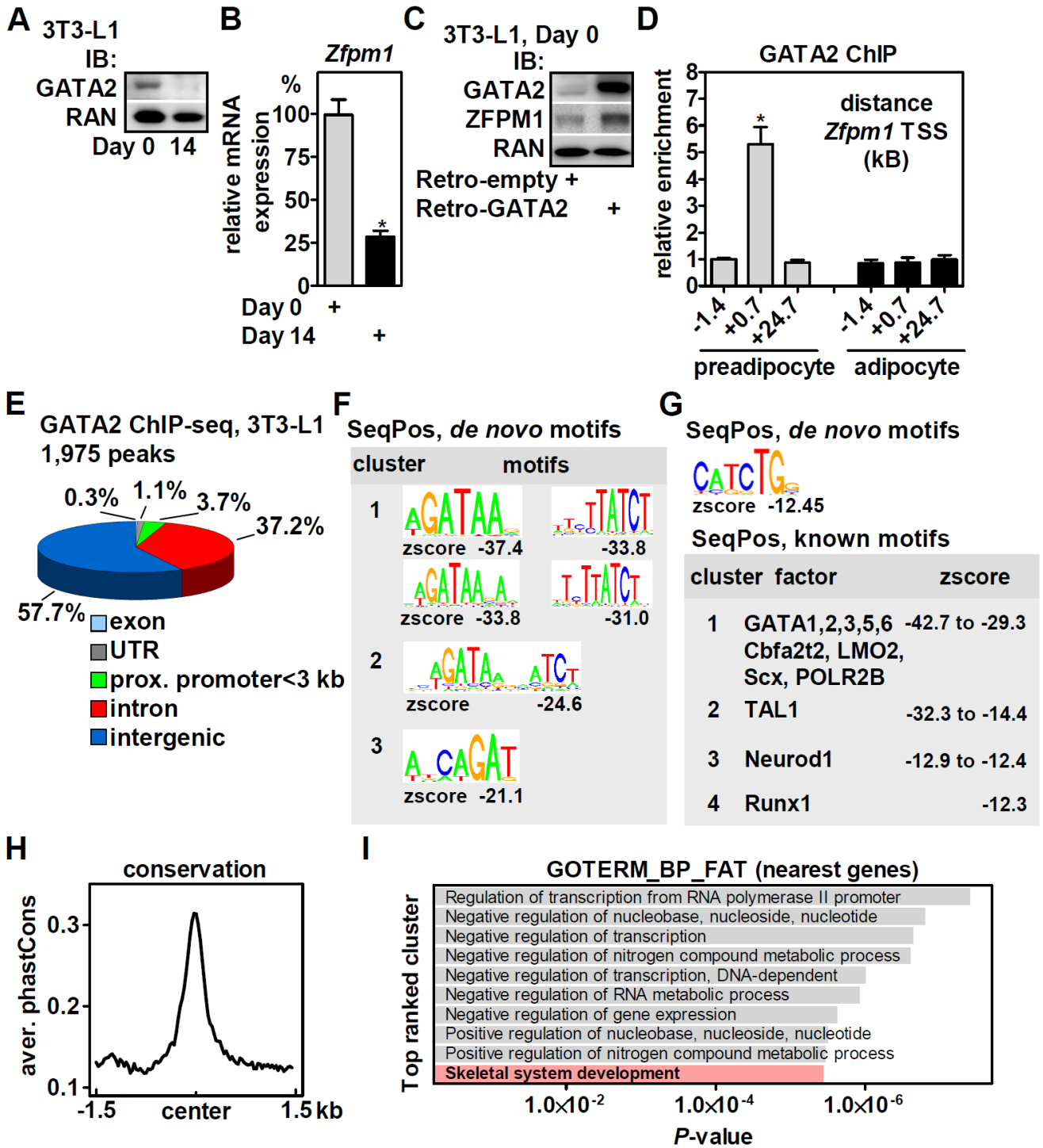

Tolkachov A *et al.* Figure 2

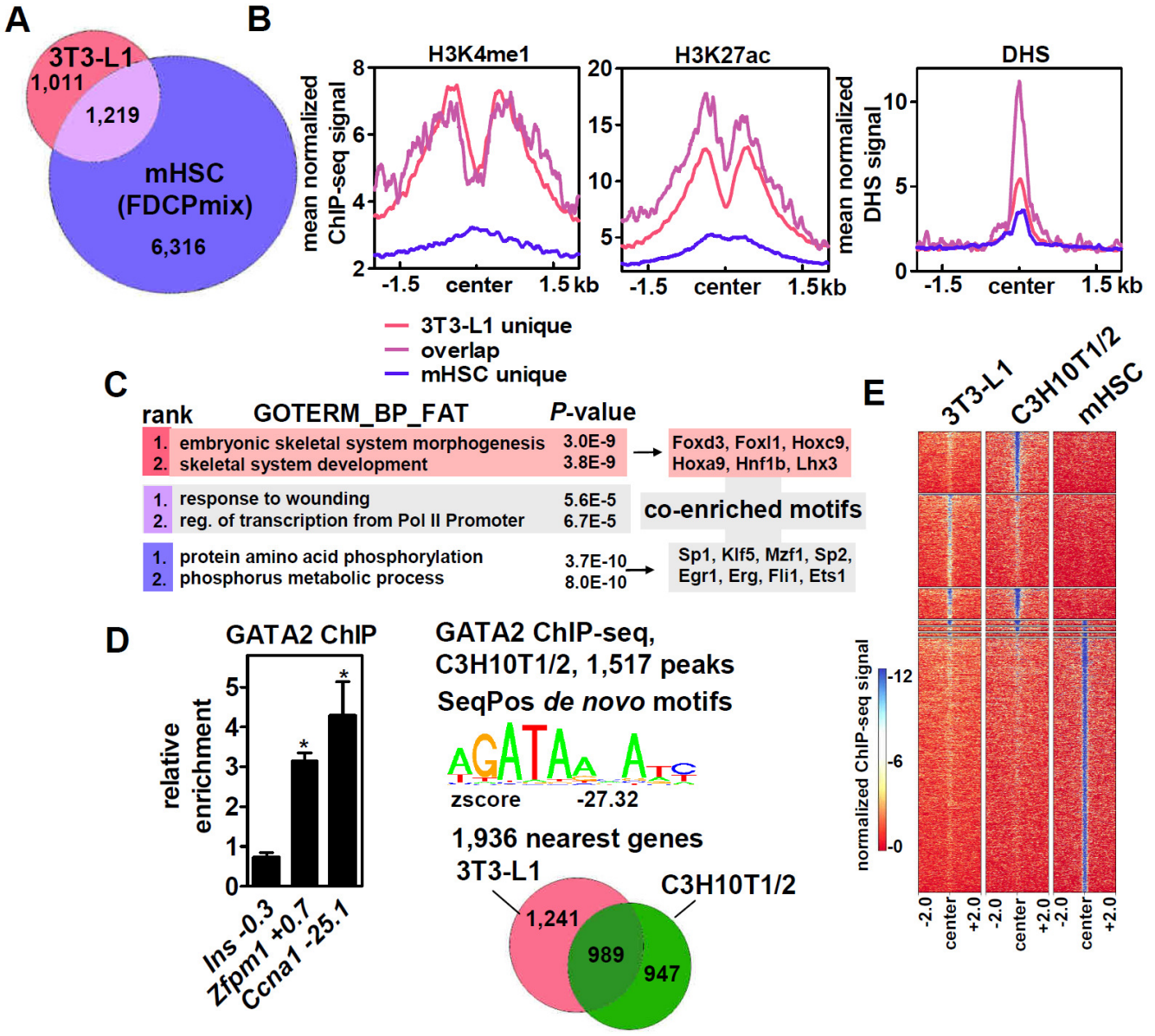

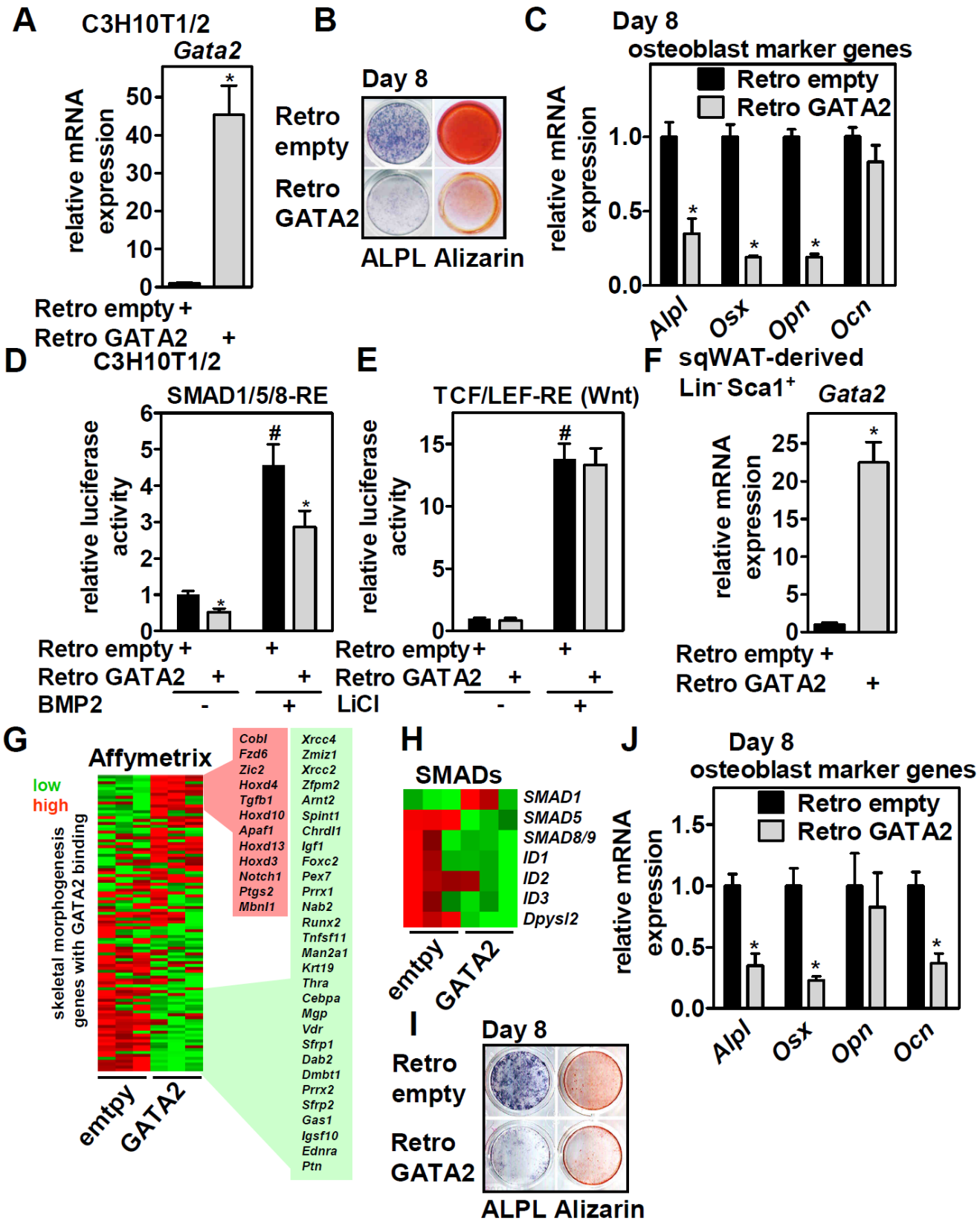

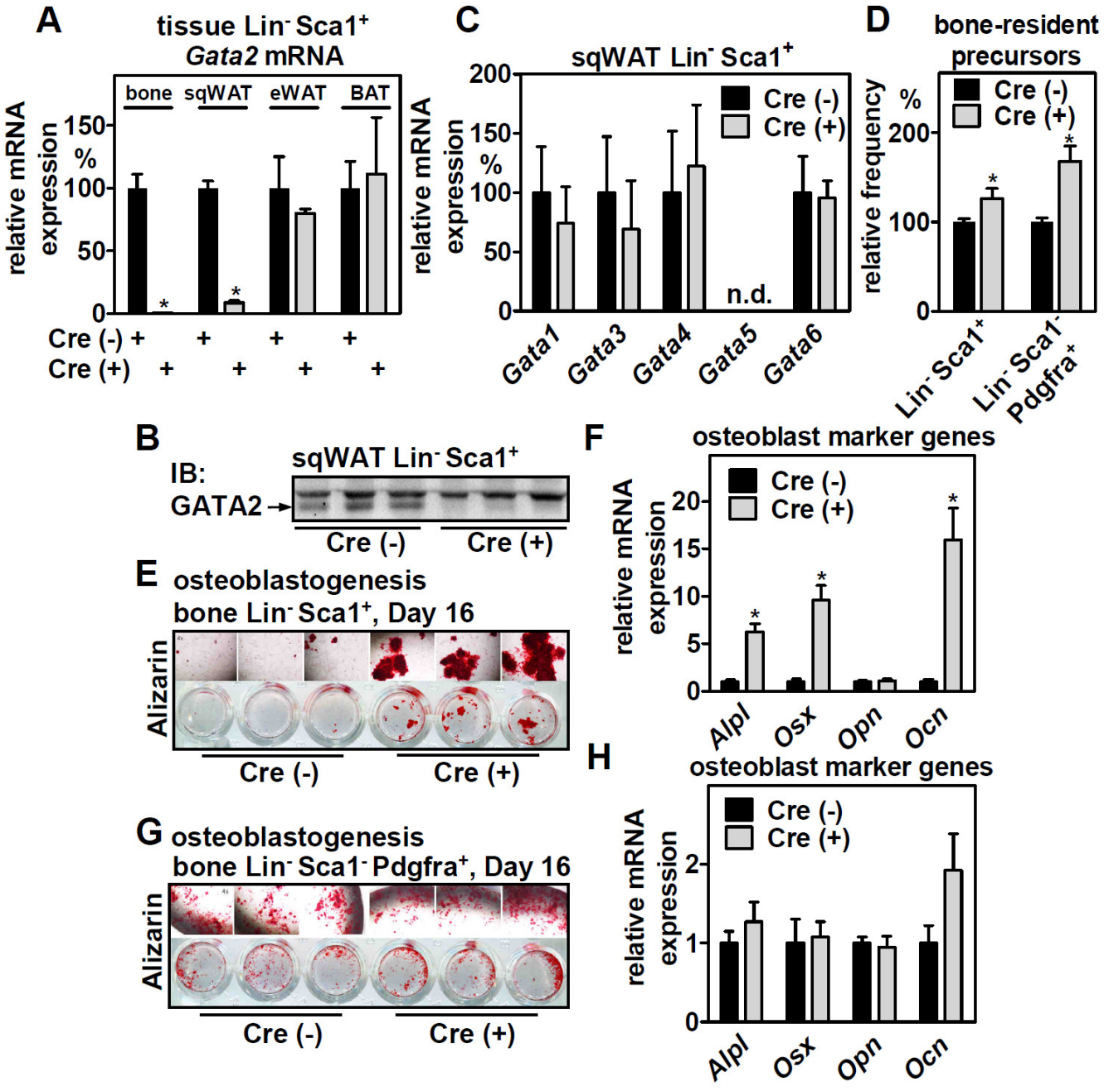

Tolkachov A *et al.* Figure 5